QUALITATIVE CALCULATIONS OF TRANSONIC DRAG-RISE CHARACTERISTICS USING THE EQUIVALENCE RULE

Y. C-J. Sedin
SAAB-SCANIA AB
S-581 88 Linköping, Sweden

Abstract

The aerodynamic drag is very important to the performance of an aircraft. The present work is to find out if and how the classical transonic equivalence rule can be used in zero-lift drag-rise calculations of configurations with moderate spanwise extensions. Some preliminary calculations of drag-rise due to lift have also been considered. The calculations were aimed at qualitative rather than quantitative answers. A number of applications are shown for real aircrafts and wind tunnel models. Results are compared with performance data and tunnel tests. The wave drag is computed by numerically solving the non-linear small perturbation equation about an equivalent axisymmetric body.

1. INTRODUCTION

Aerodynamic drag is one of the most important quantities to get hold of in the early phase of a new aircraft project. It is also one of the most difficult parameters to predict especially in the transonic flight regime. Drag has an immediate impact on speed, range and fuel consumption. Simple and inexpensive computational tools are therefore of great engineering value. An example of such a theoretical tool is the classical transonic area rule with special reference to the wave drag.

The basis of the area rule with zero lift was experimentally laid by Whitcomb[1] and theoretically by Oswatitsch and Keune[2]. In recent years this classical rule has been extended to lifting configurations by Cheng and Hafez[3] and Barnwell[4].

The transonic flight envelope has gained a renewed interest during the last years, which is reflected in the almost explosive development of new numerical techniques for calculating various transonic flow problems. Today there exists a whole scale of methods[5] with different degrees of sophistication. At the upper end we have computer programs for solving wing-body problems[6]-[7]. However, in most cases the body is still rather crudely modelled and to improve on this is usually costly due to the complicated geometry involved. The complex geometry requires perhaps many hundreds of thousands of grid points in the computational domain to get a good resolution with a finite difference method. In the light of this, simple equivalence rules dealing with equivalent bodies of revolution still play an important role in the preliminary design stage where all the close details of an aircraft are not known or even considered.

The present paper is a more or less complete summary of the work that has been conducted at SAAB-SCANIA to find out if and how the classical transonic equivalence can be used in zero-lift drag-rise calculations. The considered configurations mostly have a moderate spanwise extension typical to fighter-type aircrafts. Some preliminary calculations of drag-rise due to lift have also been performed. The aim was set to qualitative rather than quantitative answers, though surprisingly many cases show the latter. A number of applications are given for real aircrafts and wind tunnel models. Results are compared with performance data and tunnel tests. The wave drag is numerically computed by solving the non linear small perturbation equation about equivalent axisymmetric bodies. The finite difference method used is that developed by Berndt-Sedin-Karlsson[8-10]. Subsonic freestream Mach numbers including unity are being considered.

The presented results have been collected sporadically during the last five years. It is felt, however, that the findings still have news value to a broader public and that impulses might be given to fresh research within this area. The numerical results are related rather straight forward and no deeper attempt is here made to do any theoretical analyses of the consequencies. This will be left to a possible follow on of this paper.

2. BASIC EQUATIONS

2.1 Conservation laws

For steady non-viscous flow the basic physical laws may be compiled in the following equations

- Mass flux : $\mathrm{div}(\rho\bar{V}) = 0$ (1)
- Momentum flux: $\mathrm{DIV}(\rho\bar{V}\bar{V} + p\bar{\bar{I}}) = 0$ (2)
- Energy flux : $\mathrm{div}(\rho\bar{V}(\frac{1}{2}\bar{V}^2 + h)) = 0$ (3)

The symbol ρ denotes the density, p the pressure and $\bar{V}$ is the velocity. The enthalpy h is given by the relations

$$h = \frac{\gamma}{\gamma-1}\frac{p}{\rho} = \frac{a^2}{\gamma-1} = c_v \cdot T \qquad (4)$$

where γ is the specific heat-ratio c_p/c_v, a is the speed of sound and T the temperature. $\bar{\bar{I}}$ is the identity tensor and $\bar{V}\bar{V}$ is the dyadic product of the velocities. Thus equations (1)-(3) relate the divergence of vector and tensor fluxes.

The benefits of writing the laws in the form of system (1)-(3) are that relations across discontinuity surfaces are implicitly included and can readily be obtained through flux considerations over surfaces of closed control volumes. This lead for instance to the Rankine-Hugoniot relations and the shock polar expression in the case of a shock wave and to a continuous pressure across a vortex sheet. The appropriate field solution of system (1)-(3) is selected through the kinematic tangency flow condition along the concrete surface of the flying object leading to

$$\bar{V} \cdot \bar{n}_B = 0 \qquad (5)$$

The unit vector $\bar{n}_B$ is perpendicular to the body or the wing surfaces. At upstream and midstream infinity the flow is undisturbed.

2.2 Body forces

The resultant body force $\bar{F}$ exerted of the fluid, which starts with a uniform freestream $\bar{V}_\infty$ at upstream infinity, can now be obtained applying Gauss' flux theorem to a control volume enclosing the flying body and the appearing discontinuity surfaces.

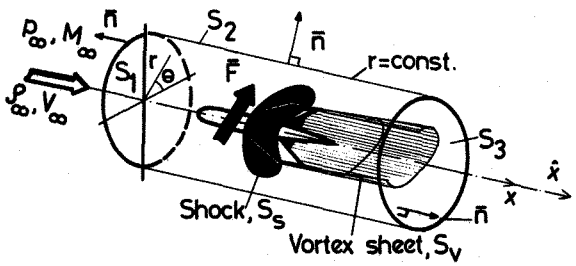

Fig 1. CONTROL VOLUME

Using equations (1), (2) and condition (5) with notations of Fig 1 will give the force $\bar{F}$.

$$\bar{F}=-\oint_{S=S_1+S_2+S_3} ((p-p_\infty)\bar{n} + \rho(\bar{V}-\bar{V}_\infty)(\bar{V}\cdot\bar{n}))dS \qquad (6)$$

Here, $\bar{n}$ is the out-leading normal vector to the surface S of the considered control volume. The shock and the vortex sheet do not contribute explicitly to relation (6) if there are no sources of mass, momentum or energy in the field. The jump conditions over the shock(s) are then given by

$$[\rho(\bar{V}\cdot\bar{n}_S)]_S = 0 \qquad (7)$$

$$[\rho\bar{V}(\bar{V}\cdot\bar{n}_S) + p\,\bar{n}_S]_S = 0 \qquad (8)$$

$$[\tfrac{1}{2}\bar{V}^2 + h]_S = 0 \qquad (9)$$

Here $\bar{n}_S$ denotes the unit vector normal to the shock and $\bar{n}_S$ is defined positive in the direction of flow on both sides of the shock wave. The brackets, $[\ ]_S$, indicate the differences between the states in front of and behind the shock. The condition across the wing vortex sheet, which also is a stream surface, will be that of a continuous pressure leading to

$$[p]_V = 0$$

The drag, D, is found by the projection of $\bar{F}$ onto the freestream direction x.

2.3 The structure of drag in a slightly perturbed flow

Taking the scalar product of eq (6) by the freestream velocity $\bar{V}_\infty$, we arrive at the following relation

$$DV_\infty = -\oint_S ((p-p_\infty)(\bar{n}\cdot\bar{V}_\infty) + \rho((\bar{V}-\bar{V}_\infty)\cdot\bar{V}_\infty)(\bar{V}\cdot\bar{n}))dS \qquad (10)$$

This is an estimation of the power we have to spend to drag the body at a speed of V_∞ through the fluid at rest. In order to split the drag in parts of wave and lift-dependent drag it is necessary to apply the second law of thermodynamics, which defines the entropy s. Now, by using the energy flux conservation eq (3) in combination with eq (1) and upon adding and subtracting a term $(\frac{p-p_\infty}{\rho})$ $(\bar{V}\cdot\bar{n})$ the following balance of energy fluxes will result

$$\oint_S ((h-h_\infty - \frac{p-p_\infty}{\rho}) + \tfrac{1}{2}(\bar{V}^2 - \bar{V}_\infty^2) + \frac{p-p_\infty}{\rho})\rho\bar{V}\cdot\bar{n}\ dS=0 \qquad (11)$$

For a flow which differs only slightly from that of a uniform freestream the second law of thermodynamics may be approximated with the difference form

$$T_\infty (s-s_\infty) \approx h-h_\infty - \frac{p-p_\infty}{\rho} \qquad (12)$$

where s is the entropy and T_∞ the freestream temperature. If eq (11) is added to eq (10) and use is made of relation (12) the approximate drag integral comes out to be

$$\frac{D}{\rho_\infty V_\infty^2} = \frac{T_\infty}{V_\infty^2}\oint_S (s-s_\infty)\frac{\rho}{\rho_\infty}\frac{\bar{V}\cdot\bar{n}}{V_\infty}dS + \oint_S (\tfrac{1}{2}(\frac{\bar{V}-\bar{V}_\infty}{V_\infty})^2\frac{\rho}{\rho_\infty}\frac{\bar{V}\cdot\bar{n}}{V_\infty}$$

$$+ \frac{p-p_\infty}{\rho_\infty V_\infty^2}(\frac{\bar{V}-\bar{V}_\infty}{V_\infty})\cdot\bar{n})dS$$

The first integral constitutes the entropy flux out of the control surface S and this is equal to the total production of entropy across all shockwaves ,S_S, within the considered volume. Thus we finally end up with the drag formula of Oswatitsch[11].

$$\frac{D}{\rho_\infty V_\infty^2} = \frac{T_\infty}{V_\infty^2}\oint_{S_S}[s]_S\frac{\rho}{\rho_\infty}\frac{\bar{V}\cdot\bar{n}_S}{V_\infty}dS_S + \oint_S (\tfrac{1}{2}(\frac{\bar{V}-\bar{V}_\infty}{V_\infty})^2\frac{\rho}{\rho_\infty}\frac{\bar{V}\cdot\bar{n}}{V_\infty}$$

$$+ \frac{p-p_\infty}{\rho_\infty V_\infty^2}(\frac{\bar{V}-\bar{V}_\infty}{V_\infty})\cdot\bar{n})dS \qquad (13)$$

Here is $\tfrac{1}{2}\rho_\infty V_\infty^2$ equal to the dynamic freestream pressure. The first integral can be estimated for weak shock waves, $[s] << c_v$, by expanding the gasdynamic relation

$$e^{\frac{(s-s_\infty)}{c_v}} = (\frac{p}{p_\infty})\cdot(\frac{\rho}{\rho_\infty})^{-\gamma} \qquad (14)$$

in perturbation velocities u, v, w on each side of the shock. Cylindrical coordinates (x,r,θ) and a cylindrical control volume are assumed according to Fig 1. The velocity vector $\bar{V}$ is equal to

$$\bar{V} = V_\infty((1+u)\hat{x} + v\hat{r} + w\hat{\theta}) \qquad (15)$$

The shock jump relations eqs (7)-(9) in combination with eqs (14) and (15) will thus give the result for small disturbances so that

$$\frac{T_\infty}{V_\infty^2}\iint_{S_s}[s]_s\frac{\rho}{\rho_\infty}\frac{\bar{V}\cdot\bar{n}_s}{V_\infty}dS_s \approx -\frac{(1+\gamma)}{12}\cdot\frac{1}{M_\infty^2}\iint_{S_s}[u]_s^3\,dS_3 \tag{16}$$

To estimate the last integral of eq (13) is more intricate, especially as the far downstream surface S_3 is passed through by an entropy wake coming from the shocks. However we will here assume (to some extent) that crossflow velocities dominate over axial perturbations. We will then proceed with our somewhat heuristic approach by saying that a fairly good approximation of the pressure is found in the following form of Bernoulli's equation

$$p-p_\infty \approx -\rho_\infty V_\infty^2\,(u+\tfrac{1}{2}(v^2+w^2)) \tag{17}$$

If the upstream- and downstream surfaces S_1 and S_3 are placed sufficiently far away from the flying object and the approximations (16) and (17) are put into the drag integral (13), the following basic structure of the drag will come out for slightly perturbed flows

$$\frac{D}{\rho_\infty V_\infty^2} = -\frac{(1+\gamma)}{12}\frac{1}{M_\infty^2}\iint_{S_s}[u]^3\,dS_3 - \iint_{S_2}uv\,dS_2 + \tfrac{1}{2}\iint_{S_3}(v^2+w^2)\,dS_3 \tag{18}$$

The symbol M_∞ deonotes the free stream Mach number. If the control volume is allowed to increase without limit the integral over the surface S_2 will go to zero and the drag will then be

$$\lim_{S_2,S_3\to\infty}\frac{D}{\rho_\infty V_\infty^2} = -\frac{(1+\gamma)}{12}\frac{1}{M_\infty^2}\iint_{S_s}[u]_s^3\,dS_3 + \tfrac{1}{2}\iint_{x=\infty}(v^2+w^2)\,dS_3 \tag{19}$$

The first integral is termed the wave drag while the second includes the classical induced liftdependent drag, due to the trailing vortex sheet behind a wing. It should be noticed that the small disturbance assumption will be violated if supersonic to subsonic shocks are assumed to exist at freestream Mach numbers too far below unity. In this case the necessary velocity perturbations would be too large to locally reach sonic or supersonic conditions. Thus we may expect the wave drag estimation to be valid only in transonic small perturbation flow.

2.4 An isentropic model of drag in transonic flow

In this section we will look at the possibilities of calculating the drag by simply assuming an irrotational velocity field $\bar{V}$ and then expanding the isentropic pressure and density relations in terms of the perturbation velocity components u,v,w. These expansions will be introduced into the mass, and momentum conservation laws of eqs (1) and (2), after having reformulated them into surface integrals.

The assumption of an irrotational flow can be expressed in cylindrical coordinates (x,r,Θ) with unit orthogonal vectors $\hat{x}$, $\hat{r}$, $\hat{\theta}$ according to

$$\mathrm{curl}\bar{V} = V_\infty\left(\frac{1}{r}((rw)_r - v_\theta)\,\hat{x} + \left(\frac{1}{r}u_\theta - w_x\right)\hat{r} + (v_x - u_r)\hat{\theta}\right) \approx 0 \tag{20}$$

The velocity $\bar{V}$ is defined in eq (15). The isentropic relations of p and ρ are found in terms of the velocity by integrating the energy-equation (3) along streamlines and combining this with the relations of eqs (4) and (14), while assuming the entropy to be a constant, $s=s_\infty$. After having done all this, we will come out with the following expansions up to the order of triple products in the perturbation velocities u,v,w

$$\frac{p}{p_\infty} = 1-\gamma M_\infty^2 u - \frac{\gamma}{2}M_\infty^2(1-M_\infty^2)u^2 - \frac{\gamma}{2}M_\infty^2(v^2+w^2) + \tfrac{1}{2}\gamma M_\infty^4\left(1-\frac{1}{3}(2-\gamma)M_\infty^2\right)u^3 + M_\infty^4 u\,(v^2+w^2) + \cdots \tag{21}$$

$$\frac{\rho}{\rho_\infty} = 1-M_\infty^2 u - \tfrac{1}{2}M_\infty^2(1-(2-\gamma)M_\infty^2)u^2 - \tfrac{1}{2}M_\infty^2(v^2+w^2) + \tfrac{1}{2}(2-\gamma)M_\infty^4\left(1-\frac{1}{3}(3-2\gamma)M_\infty^2\right)u^3 + \tfrac{1}{2}(2-\gamma)M_\infty^4 u(v^2+w^2) + \cdots \tag{22}$$

The important mass flux density $\rho\bar{V}$ comes out to have the following vector components in the $\hat{x}$, $\hat{r}$ and $\hat{\theta}$ directions

$$\frac{\rho\bar{V}\cdot\hat{x}}{\rho_\infty V_\infty} = 1+(1-M_\infty^2)u-\tfrac{1}{2}M_\infty^2(3-(2-\gamma)M_\infty^2)u^2-\tfrac{1}{2}M_\infty^2(v^2+w^2) - \tfrac{1}{2}M_\infty^2\left(1-2(2-\gamma)M_\infty^2\left(1-\frac{1}{6}(3-2\gamma)M_\infty^2\right)\right)u^3 - \tfrac{1}{2}M_\infty^2(1-(2-\gamma)M_\infty^2)u(v^2+w^2) + \cdots$$

$$\frac{\rho\bar{V}\cdot\hat{r}}{\rho_\infty V_\infty} = v-M_\infty^2 uv-\tfrac{1}{2}M_\infty^2(1-(2-\gamma)M_\infty^2)u^2 v - \tfrac{1}{2}M_\infty^2(v^2+w^2)v + \cdots$$

$$\frac{\rho\bar{V}\cdot\hat{\theta}}{\rho_\infty V_\infty} = w-M_\infty^2 uw-\tfrac{1}{2}M_\infty^2(1-(2-\gamma)M_\infty^2)u^2 w - \tfrac{1}{2}M_\infty^2(v^2+w^2)w + \cdots \tag{23}$$

To perform the necessary ordering of the different terms we will concentrate on the massflow conservation, eq (1), and the irrotationality of $\bar{V}$ expressed in eq (20). To this end we need the scaling quantities 1, l_c and ε so that

$$x \sim 1, \; r \sim l_c$$

$$v, w \sim \varepsilon \quad (\varepsilon << 1)$$

where 1 is a characteristic length of the body and l_c is a characteristic length of the cross-flow interaction. The small parameter ε is a characteristic measure of the streamline inclinations usually coupled in some way to the linearized boundary condition of eq (5).

Physically we know that the mass flux density $|\rho\bar{V}|$ has a fairly flat maximum at the local Mach number M=1. If the freestream then is transonic, $M_\infty \sim 1$, there will be a very strong and nearly incompressible lateral interaction from the stream tube area changes enforced by the presence of the body. This is also obvious from eq (23). However, at large lateral distances from the flying object the axial interaction, involving the velocity u, has to be retained to balance the lateral influence from v and w, otherwise infinite pressure would result at the body. This indicates that l_c should be fairly large and increase as $\varepsilon \to 0$, $M_\infty \to 1$, if a uniform and globally correct behaviour is sought.

When the scaling quantities are introduced into the cross-flow part of $\mathrm{curl}\bar{V} \approx 0$, eq (20) it follows that $u \sim \varepsilon l_c/l$. To properly order the mass flux density eq (23) we have to keep at least both the u- and u^2-term of the x-component. This is necessary in order to get a maximum flux when the approximate local Mach number reaches one. Thus letting the divergence operator, div ( ), operate on (23) with the assumed scalings, the following first order structure will appear

$$(1-M_\infty^2)\frac{l_c}{l^2}\varepsilon \sim M_\infty^2(3-(2-\gamma)M_\infty^2)\frac{l_c}{l^3}\varepsilon^2 \sim \frac{\varepsilon}{l_c}$$

For our purpose it is here sufficient to recognize that we may choose

$$\frac{l_c}{l} \sim \varepsilon^{-1/3}, \quad (1-M_\infty^2) \sim \varepsilon^{2/3} \qquad (24)$$

in the limit $\varepsilon \to 0$, $M_\infty \to 1$. Thus on an outer scale $l_c \sim 1 \cdot \varepsilon^{-1/3}$, we may sum up the order of the velocities to be

$$u \sim (1-M_\infty^2) \sim \varepsilon^{2/3}, \; v \sim \varepsilon, \; w \sim \varepsilon \qquad (25)$$

Now we have the tools to estimate the drag in an "isentropic model" of flow.

Through the irrotationality assumption we may define a perturbation velocity potential ϕ so that

$$\bar{V} = V_\infty(\hat{x} + \mathrm{grad}\,\phi)$$

$$u = \phi_x, \; v = \phi_r, \; w = \frac{1}{r}\phi_\theta \qquad (26)$$

By introducing these definitions into the mass flow density, eq (23), and then inserting this into the mass conservation eq (1), it is possible to calculate the velocity field. Jump conditions across discontinuity surface are then also allowed for in the velocities according to eq (7). From the irrotationality assumption we immediately have that the in-plane velocities are conserved across discontinuity surfaces (shocks), a fact which also follows from the "true" momentum condition eq (8). Then it is rather obvious that the vector product $\bar{V} \times \bar{n}_s$ is conserved also, where $\bar{n}_s$ is the normal to the shock. After some manipulations $\bar{n}_s$ follows so that

$$\bar{n}_s = \left(1 + \frac{[v]^2}{[u]^2} + \frac{[w]^2}{[u]^2}\right)^{-\frac{1}{2}}\left(\hat{x} + \frac{[v]}{[u]}\hat{r} + \frac{[w]}{[u]}\hat{\theta}\right) \qquad (27)$$

From (26) and (25) it turns out that $\bar{n}_s \approx \hat{x}$ to order $0(\varepsilon^{1/3})$.

The attention will now be focused onto the momentum equation (2) in order to formulate a drag integral. The in-plane part of the momentum condition (8) across a shock is already fulfilled. However, the normal condition is not satisfied in an isentropic flow model. Thus, in order to formulate an equivalent to the force integral, eq (6), we have to include all shocks in the surface of the control volume to account for the "miss-match" in momentum. If this is done together with p and ρ from eqs (21)-(22) and relation (23) is inserted in condition (7) the following first order result will appear (of order $\varepsilon^{4/3}$).

$$\frac{D}{\rho_\infty V_\infty^2} = -\iint_{S_2} uv\,dS_2 + \tfrac{1}{2}\iint_{S_3}((v^2+w^2)-(1-M_\infty^2)u^2 +$$

$$+\frac{2}{3}(\gamma+1)M_\infty^2 u^3)\,dS_3 -$$

$$-\frac{\gamma+1}{12}M_\infty^2\iint_{S_s}[u]_s^3\,dS_3 \qquad (28)$$

It should here be noticed that $M_\infty^2 = 1$ has been put at some places in the coefficients. The scaling laws (24)-(25) have been used throughout and the drag is of order $D \sim \rho_\infty V_\infty^2 l^2 \varepsilon^{4/3}$. The drag of (28) is compatible with the pressure given in eq (21) to the appropriate order so the same drag would have been obtained if the pressure had been summed up over the surface of the body. Equation (28) is essentially the same as that found by Murman and Cole[12] with a slightly different approach.

It is here interesting to note that the structure of the drag according to eq (28) is strikingly similar to that of eq (18) and that the limiting value of (28) as the control volume increases without limit ($S_2, S_3 \to \infty$) includes the same basic terms as that of eq (19). This is true under the conditions that $M_\infty \sim 1 + 0(\varepsilon^{2/3})$. For Mach numbers departing too far from unity the integrals containing the shock jumps, $[u]_s^3$, will however differ quite rapidly, which is a symptom on the break down of the small perturbation theory. The "miss-match" in the momentum condition across the "isentropic" shock makes up the drag due to the entropy jump across a weak shock.

2.5 Isentropic mass flux and the potential equation

Using the scaling laws of relations (24) and (25) the mass conservation law eq (1) may be formulated

on integral form as

$$\oint_{S_2} v(1-M_\infty^2 u)dS_2 + \oint_{S_3} ((1-M_\infty^2)u -$$

$$-\tfrac{1}{2} M_\infty^2 (\gamma+1)u^2 - \tfrac{1}{2} M_\infty^2 (v^2+w^2) \qquad (29)$$

$$- \tfrac{1}{2} M_\infty^2 (\tfrac{\gamma}{3}(2\gamma-1)-1)u^3)dS_3 = (S_1-S_3)$$

where $(S_1-S_3) \geq 0$ depending on the position of S_3. The difference S_1-S_3 is equal to the cross sectional area S_c if S_3 insersects with the body surface.

In this formulation, terms of order $\varepsilon^{2/3}$ and $\varepsilon^{4/3}$ have been included. Furthermore $M_\infty^2 = 1$ has been assumed at some places in the interior of the coefficients. The corresponding perturbation potential equation for ϕ, which is defined in relations (26), will thus be as follows

$$\frac{\partial}{\partial x}((1-M_\infty^2)u - \tfrac{1}{2} M_\infty^2 (\gamma+1)u^2 - \tfrac{1}{2} M_\infty^2 (v^2+w^2) -$$

$$- \tfrac{1}{2} M_\infty^2 (\tfrac{\gamma}{3}(2\gamma-1)-1)u^3)$$

$$+ \text{Div}\ ((1-M_\infty^2 u)(v\hat{r} + w\hat{\theta})) = 0 \qquad (30)$$

where the divergence operator Div( ) is active in cross-flow planes x=const. In a cylindrical coordinate system we have

$$u = \phi_x \ , \ v = \phi_r \ , \ w = \frac{1}{r}\phi_\theta$$

Due to the conserved in plane velocities across shocks, the condition on ϕ across a shock reads

$$[\phi]_s = 0$$

Terms of order $\varepsilon^{4/3}$ and $\varepsilon^{6/3}$ are included in eq (30). It is in principle only necessary to deal with terms of order $\varepsilon^{4/3}$ to estimate a velocity field with shock jump relations that enables us to derive the form of the last drag term in eq (28). However, for flows with fairly swept shock waves it is believed that eq (30) in full gives a more realistic behaviour. This is confirmed in ref (13) and eq (30) essentially agrees with that proposed by v.d. Voreen et al[13]. In ref (13), however, they have omitted the term $-(u^3)_x$ though (at least formally) this is as large as that of $-(v^2+w^2)_x$.

What finally remains to be done now is to check how good an approximation it really is to put $\text{curl}\bar{V}=0$. One way to do this is to use the well known Crocco equation, which relates $\text{curl}\bar{V}$ to grad (s). If this is done it comes out that $\text{curl}\bar{V} \sim [s]_s$ behind a shock, and thus we have that $\text{curl}\bar{V} \sim \varepsilon^{6/3}$. This shows that $\text{curl}\bar{V}=0$ is a fairly good approximation.

3. TRANSONIC EQUIVALENCE RULE

3.1 General background

The equivalence rule states that sufficiently far away from a slender flying object, the stream tubes enclosing the object are axisymmetrically displaced and the flow seems to have been created by an equivalent body of revolution. The question then arises how to predict and calculate the equivalent body. In the classical theory[2] the equivalent body is equal to that body which has the same cross sectional area distribution as that of the three dimensional flying object. In the near field the classical theory says that the flow differs from that of the equivalent body by a two-dimensional incompressibel crossflow which helps to fulfil the tangency flow condition along the real body surface.

The very basic assumption behind all transonic equivalence rules is that the inner field close to the body mainly is governed by lateral interactions. This gives rise to a two-dimensional incompressible Laplace equation for the potential ϕ in crossflow planes, x=const. The physical reason behind this is that the massflow density is close to its maximum value almost everywhere in the flow. Thus the flow reacts fairly stiffly upon stream tube area changes due to the body. The near flow can then be built up by source, and doublet distributions around the body cross contour. In the outer limit of the inner solution the source distribution will dominate and hence collapse into a point source. Therefore the outer flow will be axisymmetric and the inner boundary condition of the outer problem will be that of a line source, who's strength is proportional to the axial gradient dS_c/dx of the cross sectional area $S_c(x)$. The outer axisymmetric equation contains the delicate non-linear axial interaction typical to all transonic flow. In essence, this is the contents of the classical equivalence rule.

However, the classical rule is not applicable to the extreme case of a mathematical thin wing with lift. In this case the incompressible inner solution does not provide us with a source distribution coming from a physical thickness. However, by merely looking at the mass flux eq (29), we may still suspect a net streamline displacement area to be possible through the quadratic terms $-u^2$ and $-(v^2+w^2)$ caused by the compressibility corrections to the classical crossflow theory. Thus, the outer flow can be controlled through these terms, and the interactions may be estimated by the incompressible cross flow. Work along these lines have been done in ref (3) and (4), which led to an equivalence rule involving lift.

3.2 The classical equivalence rule with reference to the drag

The classical theory is built on two distinguished limits, one inner incompressible region and one outer compressible region that involves the axisymmetric non-linear flow equation. The inner region is governed by pure lateral interactions according to

$$\frac{1}{r}(rv)_r + \frac{1}{r} w_\theta = 0 \qquad (31)$$

The most commonly used outer axisymmetric equation is given by

$$\frac{\partial}{\partial x}((1-M_\infty^2)u - \frac{1}{2} M_\infty^2 (\gamma+1)u^2) + \frac{1}{r}(rv)_r = 0 \qquad (32)$$

where higher order terms of eq (30) are omitted. Assuming irrotational flow eqs (31)-(32) are equations for the potential ϕ through definitions (26). The inner solution ϕ_i of eq (31) is as follows

$$\phi_i = \psi_i(r,\theta;x) + g(x) \qquad (33)$$

Here ψ_i is the pure two-dimensional crossflow solution in planes, x=const, and g(x) is an additive function of integration, to be determined by matching to the outer solution $\phi_o(x,r)$.

Now, assuming a thickness (source) dominated situation we have the following asymptotic behaviour of ψ_i in the outer limit $r \to \infty$.

$$\psi_i \approx \frac{1}{2\pi}\frac{dS_c}{dx}\ln r \qquad (34)$$

This result is nothing else but an application of the equivalence rule. The variable $S_c(x)$ is the body cross sectional area. To show (34) we have to deal with a linearized version of the body boundary condition eq (5), assuming slightly perturbed flows including small wing and fuselage thickness slopes. The boundary condition of the outer solution in the inner limit ($r \to 0$) thus becomes

$$\lim_{r\to 0}(r\phi_{o_r}) = \frac{1}{2\pi}\frac{dS_c}{dx}$$

The unknown function g(x) in eq (33) can now be found according to

$$g(x) = \lim_{r\to 0}\left(\phi_o - \frac{1}{2\pi}\frac{dS_c}{dx}\ln r\right)$$

A uniform composite solution may be constructed by adding the inner and outer solutions and subtracting the common part. Hence we have the composite solution $\phi(x,r,\theta)$ to be

$$\phi(x,r,\theta) = \psi_i(r,\theta;x) + \phi_o(x,r) - \frac{1}{2\pi}\frac{dS_c}{dx}\ln r \qquad (35)$$

An obvious deficiency in approximation (35) is that shock waves only come in via the axisymmetric term $\phi_o(x,r)$. However, for sufficiently slender configurations with zero lift the trace of the shock is surprisingly close to that of the equivalent body and in some cases this is true even in the neighbourhood of the bodies. To calculate the drag one can of course use eq (35) to predict the surface pressure, but we will instead apply an integral formulation based on eq (28) and proceed along lines similar to those of ref (14). The aim is to relate the drag of a wing-body-tail combination to that of a simple equivalent body of revolution with the same cross sectional area, $S_c(x) << l^2$.

The considered control volume is a circular cylinder according to Fig 1. The surface S_1 is placed so far upstream that the disturbances have decayed to zero. The cylindrical surface S_2 is placed at the outer limit of the inner region, $r=R_2$. The terminating surface S_3, perpendicular to x, is placed at the end of or behind the considered body. To evaluate the drag from eq (28) we have to order the different terms on an inner scale, here given by the relations

$$x \sim l, \qquad r \sim b$$
$$v,w \sim \tau \sim \sqrt{(S_c)_{max}/l^2} \qquad (36)$$

b is for instance proportional to half the wing span and τ is an overall slenderness parameter, related to the maximum cross sectional area $(S_c)_{max}$. From the irrotationality assumption, eq (20), we get the order of u to be $u \sim \tau b/l$. In the limiting process, $\tau \to 0$, we will assume that $b/l \sim \tau^\beta$, where $\beta \geq 0$. Thus, we end up with the order $u \sim \tau^{1+\beta}$. What finally remains to be done is to order $(1-M_\infty^2)$. From outer considerations in section 2.4, eq (24), the limiting transonic process is defined by $(1-M_\infty^2) \sim \varepsilon^{2/3}$ as $\varepsilon(\tau) \to 0$. Hence the relation $\varepsilon(\tau)$ is to be found. This is most easily evaluated by requiring the inner solution (33)-(34) to have the same order of the radial velocity v as that of the outer on the radial scale $r \sim l\,\varepsilon^{-1/3}$. Thus upon taking the radial derivative of eq (34) and ordering this to the outer velocity v of relation (25), we may sum up the following results

$$\varepsilon \sim \tau^3, \quad u \sim \tau^{1+\beta}, \quad v \sim \tau, \quad (1-M_\infty^2) \sim \tau^2$$
$$\frac{b}{l} \sim \tau^\beta, \quad (\tau << 1, \quad \beta \geq 0) \qquad (37)$$

To get compatible orders of the drag integral in both the inner and outer regions we have to choose $\beta=1$. This result is also found when u is matched to the outer solution. Upon scaling eq (28) with relations (37) and $\beta=1$ the following drag integral comes out in the inner region.

$$\frac{D}{\rho_\infty v_\infty^2} = -\iint_{S_2} uv\,dS_2 + \frac{1}{2}\iint_{S_3}(v^2+w^2)\,dS_3 \qquad (38)$$

The integral over the shocks can obviously be neglected on an inner scale according to this analysis. The drag is of order $D \sim \rho_\infty v_\infty^2 \tau^4$, which agrees with the outer formulation. The first integral can be estimated by first inserting eq (34) into solution (33) and making use of definition (26). The second integral of eq (38) is further found by expanding the expression Div (ψ_i Grad ψ_i) and applying Green's theorem. The function ψ_i is the incompressible harmonic solution of eq (31) so that $v^2+w^2 = (\text{Grad}\,\psi_i)^2$. The operators Div( ) and Grad( ) are active in crossflow planes x=const. The difference between the drag D of the actual configuration and its equivalent body of revolution having the drag D_{eq} and the same area distribution $S_c(x)$ can thus be evaluated as

$$\frac{D-D_{eq}}{\rho_\infty v_\infty^2} = -\frac{1}{2}\oint_{C_B(1)}\psi_i(\text{Grad}\,\psi_i)\cdot\bar{n}_B\,ds + \frac{1}{4\pi}(S_c'(1))^2\ln R(1) \qquad (39)$$

The line integral is performed along the cross contour C_B created in the intersection between the plane S_3 and the body surface extended into any necessary auxiliary cut. The argument (1) indicates that S_3 is placed at the downstream end of the configuration and R is the radius of the equivalent body. The outleading normal $\bar{n}_B$ is perpendicular to the real and auxiliary body surface that includes C_B.

For nonlifting configurations, which end in a constant circular cylinder or a circular pointed rear body the right hand side of eq (39) would be zero.

In order not to be stuck with too complicated geometrical interpretations these conditions will be assumed in the following calculations.

3.3 Comments on the classical equivalence rule

All the analysis performed are based on small perturbations. Thus the results are not reliable if transonic effects are encountered at freestream Mach numbers too far below unity. Another remarkable fact is that the right hand side of eq (39) is independent of the freestream Mach number. Furthermore the theory must fail when the inner field is too complicated with pronounced three-dimensional transonic interactions including e.g. oblique intersecting shock waves. In such cases detailed local sub expansions are needed and the simplicity of the overall first order theory will be lost. It would then probably be better to go directly for a complete numerical solution.

Another difficulty that ought to be mentioned is that a wing-body configuration generally has two different streamwise length scales, one for the wing and one for the body. To use only one surely restricts the configuration to be geometrically nicely blended and to have a sufficiently swept wing.

The classical theory works with a lateral inner length scale according to $b \sim 1\tau$, where 1 is the undistorted streamwise scale. However, it is possible to carry out the same type of analysis on a lateral scale of order $b \sim 1$. In this case we need a new slenderness parameter δ with e.g. $\delta \sim S_{c_{max}}/(bl)$ and $b/1 \sim 0(1)$. The practical results of the lowest order analyses will be the same but the next higher order compressibility corrections to the inner crossflow equation will be quite different. The correction in the first case with $b \sim 1\tau$ is shown in the right hand side of the following relation

$$\mathrm{Div}\ (v\hat{r}+w\hat{\theta}) \approx \tfrac{1}{2} M_\infty^2 \frac{\partial}{\partial x}(v^2+w^2) + M_\infty^2\, \mathrm{Div}(u(v\hat{r}+w\hat{\theta})) \qquad (40)$$

where the left hand side (l.h.s.) is $0(1)$ and the right hand side (r.h.s.) is of order τ^2. In the second case when $b \sim 1$ we have

$$\mathrm{Div}(v\hat{r}+w\hat{\theta}) \approx -\frac{\partial}{\partial x}\left((1-M_\infty^2)u - \tfrac{1}{2} M_\infty^2 (\gamma+1)u^2 - \right.$$

$$\left. - \tfrac{1}{2} M_\infty^2 (v^2+w^2)\right) + M_\infty^2\, \mathrm{Div}(u(v\hat{r}+w\hat{\theta})) \qquad (41)$$

where l.h.s. is of order δ and r.h.s. of order δ^2. The connection between the outer parameter ε and δ is evaluated to be $\varepsilon \sim \delta^{3/2}$ and hence we have $(1-M_\infty^2) \sim \delta$ as $\delta \to 0$ with $b/1 \sim 0(1)$.

The difference between eqs (40)-(41) is that the latter contains the typical transonic non linear interaction as a correction to the inner crossflow equation. Thus we may suspect that applications of eq (39) will not be especially successful in calculating the drag for configurations where half the wing span is of order $b \sim 1$ and δ is relatively large (e.g. a thick wing).

From an engineering point of view it would be valuable to have a simple theory that at least qualitatively could give some guide lines how to distribute the physical cross sectional area in the spanwise direction to get a good drag-rise behaviour. The classical transonic area rule only deals with the total streamwise area distribution and does not tell how to blend the different parts together.

3.4 Transonic equivalence rule involving lift

The classical equivalence rule has quite recently been extended to lifting configurations by Cheng and Hafez [3] and Barnwell [4]. Their work are based on fairly complicated analyses by extensively using matched asymptotic expansions. This will not be related here. However, a few plausible comments will be stated in relation to eq (29), where the mass flux through the surfaces of a cylindrical control volume (Fig 1) is considered. What we essentially wants to see is how the net streamline displacement area, which approximately is the integral of v over S_2, varies with x when the surface $S_3(x)$ is moved downstream over the wing.

To study this, assume a plane lifting wing with zero thickness and angle of attack α. Thus the right hand side (r.h.s.) of eq (29) is zero because $S_c(x)=S_1-S_3=0$. Due to the wing circulation we have a positive velocity u above the wing plane and the same amount but negative below. Concerning the velocity v this is negative above and positive below the wing, while w is antisymmetric with respect to a vertical symmetry plane through the wing center with positive values on starboard. The magnitude of u is proportional to the streamwise gradient of the accumulated wing circulation, thus $u \sim 1 dC_L(x)/dx$ where $C_L(x)$ is the accumulated lift coefficient at station x. The crossflow velocities v, w are proportional to either the accumulated circulation or the geometrical angle of attack (or the downwash).

To sort this out we have to estimate the whole integral of $(v^2+w^2)/2$ over the surface S_3 at once. This was in fact already done in connection with the drag integral of eq (38) and the main result was the line integral of eq (39). Recalling that the potential jump across a wing is proportional to the circulation and that the tangency flow condition must be fulfilled, we may state that the kinetic crossflow integral is proportional to $\sim C_L(x)\alpha$. With all this in mind eq (29) suggests the following displacement area structure due to lift (strictly for certain planforms only).

$$S_L(x) = \iint_{S_2(x)} v\,dS_2 \sim l^2 M_\infty^2 \left(\mathrm{const}_1 l^2 \left(\frac{dC_L}{dx}\right)^2 + \right.$$

$$\left. + \mathrm{const}_2 C_L(x)\alpha\right)$$

Odd powers of u will not contribute over S_3. The first order thickness contribution to a real physical configuration is given by the r.h.s. term S_1-S_3 of eq (29). This term is of course equal to the cross sectional area $S_c(x)$. The total equivalent area S_{eq} then comes out to be

$$S_{eq}(x) = \iint_{S_2(x)} v\,dS_2 = S_c(x) + S_L(x)$$

In this we have not considered any coupling between thickness and lift. Furthermore we have to consider where to place the outer surface S_2 which requires detailed analyses.

However, the found heuristic result agrees in structure with the formula of Barnwell [4]. His equivalent body of revolution has the following area distribution

$$S_{eq}(x) = S_c(x) + \frac{\gamma+1}{2} B\pi\left(\frac{S}{4\pi}\frac{dC_L}{dx}\right)^2 +$$

$$+ \tfrac{1}{2} S C_L(x)\sin\alpha \ , \quad B = \ln\left(\frac{l^2}{b\, R_{max}}\right), \qquad (42)$$

where $C_L(x)$ is the accumulated lift coefficient and S is the reference area. The radius R_{max} is the maximum equivalent radius corresponding to $S_{c_{max}}$ and b is the wing semispan. The length scale l is not unique but it is here assumed to be the streamwise extension of the main lifting region. The theory assumes $b/l \sim 0(1)$ and $\alpha << 1$. The scale factor B is as suggested by Barnwell in ref (15).

Apart from the reference area S, the last term of eq (42) is equal to the classical induced drag coefficient of slender wings and bodies. However, in ref (3) Cheng and Hafez found that apart from S, the last term should be equal to half the induced drag coefficient at a far downstream position. Unfortunately this contradiction was discovered too late by the present author so all numerical calculations were performed using eq (42) with no further investigation concerning the last term.

The far downstream result of Cheng and Hafez in the Treffz plane is in principle deductive from eq (29) with the vortex drag component of eq (19). However the last term of eq (42) may still agree with this result if we only assume the wing to have no leading edge suction. In that case the induced vortex drag coefficient is simply the projection of the wing normal force coefficient onto the free-stream direction.

What makes eq (42) so attractive is the simple form, which enables fairly inexpensive numerical calculations to qualitatively estimate the influence by lift.

4. COMPUTATIONAL MODELS

4.1 Transonic zero lift drag-rise

The wave drag is assumed to be equal to that of the equivalent body of revolution with area $S_c(x)$. Thus the right hand side of eq (39) will be set to zero. This is strictly true for certain configurations only as was pointed out in section 3.2. However, obscure results with a constant rest drag would otherwise be possible for freestream Mach numbers close to or below the critical. We may also argue that boundary layer effects together with the outgoing jet will form a fairly constant or slowly varying section locally at the end of the configuration. The geometrical interpretation of the cross sectional area is as shown in Fig 2.

The equivalent area starts with a constant stream tube, corresponding to the ingestion of air by the intakes and ends in a constant cylinder simulating the jet from the engine.

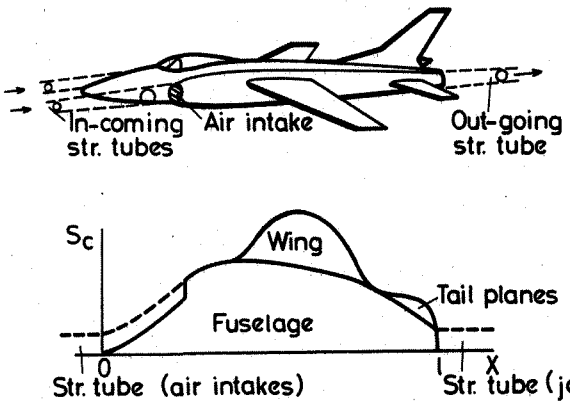

Fig 2. CROSS SECTIONAL AREA

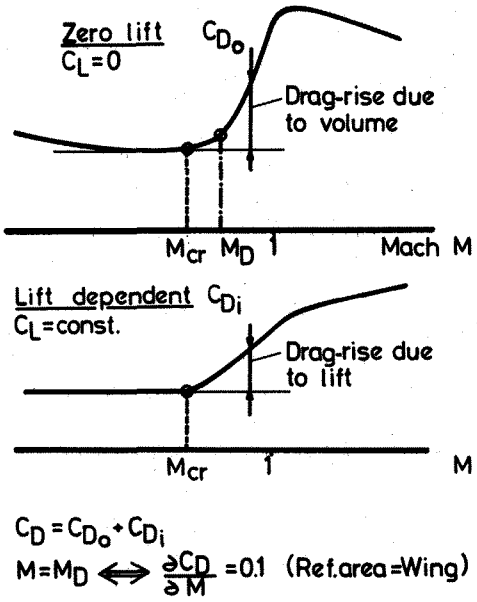

Fig 3. DRAG CHARACTERISTICS

The drag of the equivalent body was in this paper calculated by numerically solving eq (32) with the finite difference method of Berndt-Sedin-Karlsson (8-10). The number of mesh points covering the length of the body usually was about 25. In some cases a certain smoothing had to be applied to the cross sectional area $S_c(x)$. The outer boundary of the computational domain was placed at a radius of 6-8 body lengths and a far field was assigned at this boundary. The radial spacing was chosen to be logarithmic and about 60 points were used. The whole x-axis was mapped onto a finite interval and about 40 points were spent on this. The pressure was approximated according to eq (17). The drag coefficient C_D was defined by the integral

$$C_D S = \pi \int_{Body} C_p \, d(R^2)$$

$$C_p = \frac{p-p_\infty}{\frac{1}{2}\rho_\infty V_\infty^2} = -2u-v^2$$

where S is the reference area and R is the radius of the equivalent body. Special care had to be taken when numerically integrating the pressure coefficient C_p at the start and at the end of the body due to the singular behaviour there.

Typical drag-rise characteristics versus Mach number are shown in Fig 3, where M_{cr} denotes the critical freestream Mach number and M_D is the drag divergence Mach number for which $\partial C_D/\partial M_\infty = 0.1$ (ref area= wing area).

4.2 Transonic drag-rise due to lift

Preliminary studies to investigate the order of magnitudes were done using Barnwell's formula, eq (41), as this could be done in connection with a thesis by Lövgren[16]. However, in the light of eq (29) and the qualitative discussion of this in section 3.4 the lift dependent terms in eq (41) were weighted by a factor M_∞^2. Thus the equivalent body was created by adding the streamline displacement area due to lift on top of the physical area $S_c(x)$ defined in Fig 2. It is here interesting to note that far downstream the equivalent body will always end in a constant cylindrical part even if the physical body is closed. The additional downstream area is related to the classical vortex drag.

The accumulated lift coefficient $C_L(x)$ was simply estimated by linear three-dimensional theory. A vortex lattice method gave $C_L(x)$ for the wing. The wing was geometrically continued to the fuselage centerline. The lift contribution from the fuselage was neglected. The vortex panel method was checked to give the right incompressible crossflow solution in the limit $M_\infty \to 1$. Without further considerations the wave drag of the equivalent bodies were calculated with and without lift according to section 4.1. By subtraction of these results the drag-rise due to lift was defined. The calculated drag-rise due to lift was compared with wind tunnel experiments where the experimental data first were corrected by subtracting the experimental zero lift drag and the pure subsonic vortex drag at the specified total C_L-value (drag-rise due to lift = $C_D(M_\infty, C_L) - C_{D_o}(M_\infty) - C_{D_i}(M_{cr}, C_L)$).

5. NUMERICAL RESULTS AND DISCUSSIONS

5.1 Zero-lift drag-rise

Fig 4 illustrates a test case for the numerical procedures to calculate the drag of an axisymmetric body. Two parabolic arc bodies are considered, one of fineness ratio $f=6\sqrt{2}$ (Body I) and the other with f=6 (Body II). The calculated pressure distribution of body I at Mach number M=0.99 is in excellent agreement with experimental data apart from some minor differences due to viscous effects behind the shock. The viscous displacement thickness has not yet been considered in any of the present calculations. The calculated wave drag versus the free-stream Mach number is also in a very good agreement with experimental data when the viscous part of the pressure drag is subtracted from the experimental points (which include viscous pressure drag). This agreement seems to be equally good for both Body I and Body II. The experiments were carried out by Drougge[17].

Figures 5-10 show computed drag-rise curves of equivalent bodies to a number of aircrafts and wind tunnel models. The calculated data are compared with wind tunnel experiments, flight-tests and performance data. The latter are data used for performance calculations and these data are assumed to be the "best" synthesis between flight-tests and wind tunnel experiments. Some geometrical parameters of the presented configurations are given in Table 1.

Fig	Type	τ	τ_w	$\tau_w(\frac{b}{l_w})\cdot(\frac{b}{l})^2$	$\tau_w\cdot(\frac{b}{l})^3$
5	Wt-model	.121	.060	.0059	.0030
6	AJ37	.131	.040	.0024	.0016
6	A32	.152	.090	.0194	.0071
7	J35	.135	.050	.0023	.0018
8	F5	.103	.050	.0046	.0012
9	Hunter	.132	.085	.0099	.0041
10	J29	.214	.110	.0367	.0133

Table 1. CONFIGURATION PARAMETERS

The symbol τ denotes the relative thickness based on the maximum cross sectional area (with the intake areas subtracted) and the total configuration length l. The notation τ_w is the relative airfoil thickness of the wing, while b is the wing semi-span and l_w the overall length of the wing in the stream-wise direction. The last two groupings of parameters are attempts to a rough ordering of how axisymmetric the inner crossflow solution is on an outer length scale proportional to $r \sim 1/\tau$. They are constructed by considering the quadrupole term of the outer expansion of the incompressible inner solution. The first group is connected with the periferical variation in the axial disturbance velocity, while the second is related to the same variation in the radial velocity. Both quantities are approximately normed by the symmetric source contribution.

Looking through the figures 5-10 we may generally say that there is a qualitative agreement between calculated and "true" drag except for the case with the SAAB J29 "Tunnan", which is a fairly thick and wide aircraft. In some cases we can also claim a rather decent quantitative description as in the cases with the SAAB AJ37 "Viggen", the SAAB J35 "Draken" and the Northrop "F-5". However, when it comes down to calculate the drag divergence Mach number M_D, as defined in Fig 3, things are more complicated and the requirements on the quantitative accuracy may become fairly sharp to get a good estimate. Figure 11 gives a picture of correlation between the "true" M_D and the calculated $M_{D_{calc}}$. From this limited sample of cases (16 points) it seems as if a rather good prediction can be obtained when the Mach number M_D is in the order of 0.9. Locally in this region the prediction errors in M_D lies approximately within $\pm$ 0.015. For Mach numbers below 0.9 the method is conservative and for values above 0.9 (towards unity) M_D is over-predicted. For project work up to now the method has simply been empirically calibrated by drawing a line through the sample of points. The corrected method has successfully been used in preliminary design work at Mach numbers below 0.9. However, a non-critical use is not recommended.

The data which the calculated results are compared

to are mostly taken from unpublished sources. However, the wind tunnel tests of Fig 6 are due to Whitcomb[1] and the flight tests of Fig 9 is found in ref (18). Concerning wind tunnel tests, it usually is so that the Reynolds' number is too low which can inflict on the shock-boundary layer interaction giving results that are different from full scale data. The viscous effects can also be quite different in the equivalent body case compared to the three-dimensional situation. To separate drag and thrust in real flight tests is also rather difficult especially as most evaluation techniques are dependent on some a priori information about the engine.

In the present applications of the equivalence rule we have not considered any viscous displacement effects. The theory itself is built on small perturbation assumptions so if transonic flow occur at too low free-stream Mach numbers, these assumptions will be violated. To examplify this, we will approximately need an axial super velocity that is about 62 % of the free stream to locally reach a Mach number of M=1.02 in a flow with a free stream Mach number of M_∞=0.7. However, to locally reach M=1.02 from M_∞=0.9, we only need about a 12 % increase in velocity over the free stream. The very basic assumption behind the equivalence rule is that the stream-wise interaction can be neglected compared to the lateral cross-flow in the neighbourhood of the flying object. This incompressible inner approximation is good for configurations with small slenderness ratios and becomes better when the local Mach number is fairly close to unity almost everywhere in the flow near the body. The inner cross-flow solution tends to an axisymmetric one far away from the actual body cross-section. However, it has to approach this sufficiently fast in order to meet the outer axisymmetric transonic solution on a radial scale mainly determined by the length and the slenderness of the equivalent body. This surely puts some restrictions on how much a configuration can be extended in the spanwise direction in terms of wing cross-sectional area, semi-span and wing-sweep to fall within the applicability of the classical transonic equivalence rule.

The deviations in Fig 11 between the "true" drag divergence Mach number and the calculated one are certainly due to some of the mentioned restrictions on the theory. The SAAB J29 "Tunnan" in Fig 10, for instance, is a typical example of a configuration which is too thick and too wide. The average (local) Mach number in the close neighbourhood is probably also subsonic and too far from unity (at least in the beginning of the drag-rise phase). The same argument can presumably also be used to explain some of the deviations in drag-rise Mach numbers for Mach numbers close to one in Fig 11. In these cases the average (local) Mach number will probably be on the supersonic side, thus reversing the correlation compared to the situation in Fig 11 for Mach numbers roughly below 0.9. This behaviour may also be explained by interpreting the stream-wise interactions in terms of spatial source and sink distributions in cross-flow planes. The source and sink distributions, which make up the errors in the inner slender-body approximation, depend on how much subsonic and supersonic flow there is in the flow.

To round off this section, we may say that the experiences so far seem to indicate that aircrafts which are good for a drag-divergence Mach number of about 0.9 usually are enough slender and compact to fit into the classical transonic equivalence rule (with reference to drag as interpreted in this paper). To get outside this narrow Mach number range the theory needs to be improved in scope and quality. Such an improved theory would probably also be able to give some guide-lines how to distribute the cross-sectional area in the span-wise direction to get a low drag. One step in that direction was in fact already taken by Berndt[19], who considered the isolated Mach one case.

5.2 Drag-rise due to lift only

Preliminary calculations of the drag-rise due to lift only were performed by Lövgren[16] according to outlines given in section 4.2. Some results of these computations are shown for two configurations in Fig 12-13. The wing, which is the same for both configurations, is of an advanced transonic design that was derived at Saab-Scania. The total area distribution at zero-lift in Fig 12 was especially designed to have a low transonic drag and it was constructed out of an ellipsoid that was distorted at the rear end. The zero-lift area distribution of the configuration in Fig 13 was found by mounting the wing on a fuselage with a cylindrical mid-section and a pointed ogive nose. The maximum cross-sectional areas of the two configurations in Fig 12 and Fig 13 are the same. The additional area distribution due to a lift coefficient of C_L=0.3 and a free-stream Mach number of M=0.9 is indicated in both figures.

The calculated drag-rise contributions due to lift only are plotted versus the free-stream Mach number at C_L=0.3 in Fig 12 and 13. The agreement between calculations and wind tunnel experiments is surprisingly good. The scattering in the experimental points are caused by tunnel induced vibrations in the model.

Several other cases with other configurations have been calculated with about the same quantitative agreement as in Fig 12-13. However, before drawing any extensive conclusions about the method, we have to bear in mind the comments stated at the end of section 3.4, concerning the far downstream contribution to the cross-sectional area (coming from the vortex wake).

5.3 Perspective on the classical zero-lift composite solution

To get a close view of the classical matched asymptotic solution, according to eq (35) in section 3.2, some pressure distributions of a number of configurations were calculated in a thesis by Karlsson[20]. Figure 14 shows a swept wing-body combination, where the radius of the equivalent body is proportional to the shape function $((x/l)-(x/l)^n)$ with n=3.39. The airfoil is a symmetric parabolic arc and the free-stream Mach number is 0.9. The composite solution is here compared with results from a linear three-dimensional panel method (though the critical pressure obviously is exceeded). The inner incompressible cross-flow solution of eq (35) was calculated by a piece-wise constant source and sink distribution along cross-contours of the consecutive cross-sectional areas. The outer non-linear axisymmetric problem was solved by using the method by Berndt-Sedin-Karlsson[8-10]. In spite of the fact that linear theory is not applicable in this case, we may generally say that the agreement between the

pressures as computed with the two methods is astonishingly good. However, it seems as if the composite solution reacts more stiffly upon the waisted midpart of the fuselage. The trace of the axisymmetric configuration shock, which appears in the composite solution, does not hit the wing but lies slightly behind. In a "true" non-linear three-dimensional solution we would have expected a shock wave to appear somewhere at the rear part of the wing and to be fairly strong in the tip region.

A similar calculation at Mach one of a delta wing-body combination is shown in Fig 15. In this case the composite solution is compared with the classical method of local linearisation as applied in ref (21) by Spreiter and Stahara. The equivalent body, which is 10 % thick, is of the same shape as the former configuration. The wing airfoil is a symmetric parabolic arc, 4 % thick. Even in this case the composite solution agrees very well with the method of comparison apart from the positive pressure increase behind the configuration shock, which ref (21) does not catch. The trace of the shock wave, coming from the axisymmetric outer solution, seems to be in a realistic position at the end of the wing. It is known from experiments[1] that the shock originating from the equivalent body of revolution lies fairly close to the three-dimensional situation even in the neighbourhood of the configuration when this is sufficiently slender and compact.

6. CONCLUDING REMARKS

The aim of the present study was to investigate if and how the classical equivalence rule could be used in zero-lift drag-rise calculations of fighter-type aircrafts. It was then found that qualitative and in many cases also quantitative drag-rise characteristics usually can be expected for configurations that are slender and compact enough to have a drag-divergence Mach number in a narrow region around Mach 0.9. For such configurations it seems possible to predict the drag-divergence Mach number to within ± 0.015 when viscous effects are not too pronounced. Not unexpectedly, the theory was most confined to compact configurations of moderate spanwise extensions such as delta wing-body combinations. An empirical-statistical correction of the theory has successfully been tried for engineering purposes to extend the applicability of the Mach number range. However, a non-critical use of such a corrected method is not recommended without detailed insights into the consequencies of the break down of the theory. An improved theory (or a qualitative error estimate if that is possible) would probably give qualitative guide-lines how to distribute the cross-sectional area also in the spanwise direction to get a good drag-rise behaviour. However, an improved method must still be economically competitive to be justified in practical early design work.

The preliminary calculations of drag-rise due to lift, which have been conducted so far, have shown surprisingly good qualitative and quantitative results. Several other examples than those presented in this paper have been computed with about the same results. However, it is felt that the drag model, as interpreted in this paper, has to be reviewed once more before any far reaching conclusions can be drawn.

7. REFERENCES

1 Whitcomb, R. T., "A Study of the Zero-Lift Drag-Rise Characteristics of Wing-Body Combinations Near the Speed of Sound," Rept. 1273, 1956, NACA.

2 Oswatitsch, K. and Keune, F., "Ein Äquivalenzsats für Nichtangestellte Flügel Kleiner Spannweite in Schallnaher Strömung," Zeitschrift für Flugwissenschaften, Vol. 3, No. 2, 1955.

3 Cheng, H. K. and Hafez, M. M., "Transonic equivalence rule: a nonlinear problem involving lift," J. Fluid Mech. (1975), vol. 72, pp. 161-187.

4 Barnwell, R. W., "Approximate method for calculating transonic flow about lifting wing-body configurations," NASA TR R-452, April 1976.

5 Jameson, A., "Transonic flow calculations", Computational Fluid Dyn., von Karman Inst. for Fluid Dyn., Lecture series 87, March 1976.

6 Caughey, D. A. and Jameson, A., "Numerical calculation of transonic potential flow about wing-body combinations," AIAA Paper 77-677, June 1977.

7 Boppe, C. W., "Computational transonic flow about realistic aircraft configurations," AIAA Paper 78-104, Jan. 1978.

8 Berndt, S. B. and Sedin, Y. C-J., "A numerical method for transonic flow fields," ICAS Paper 70-13, Rome, Sept. 1970.

9 Sedin, Y. C-J., "Axisymmetric sonic flow computed by a numerical method applied to slender bodies," AIAA Journal, April 1975, pp, 504-511.

10 Karlsson, K. R. and Sedin, Y. C-J., "The method of decomposition applied in transonic flow calculations," Proc. 5th Int. Conf. on Num. Meth. in Fluid Dyn., Enschede, June-July 1976, Springer-Verl., Lecture Notes in Physics, vol 59.

11 Oswatitsch, K., "Gas dynamics", Academic Press, 1956.

12 Murman, E. M. and Cole, J. D., "Insviscid drag at transonic speeds," AIAA Paper 74-540, June 1974.

13 van der Vooren, J.et al, "Remarks on the suitability of various transonic small perturbation equations to describe three-dimensional transonic flow; Examples of computations using a fully-conservative rotated difference scheme", IUTAM Symposium Transsonicum II, Göttingen, Sept. 1975, Springer-Verlag 1976.

14 Ashley, H. and Landahl, M., "Aerodynamics of wings and bodies," Addison-Wesley, 1965.

15 Barnwell, R. W., "Approximate method for calculating transonic flow about lifting wing-body combinations," Conf. on Aerodynamic Analyses Requiring Advanced Computers, NASA Langely, March 1975, NASA SP-347.

16 Lövgren, R., "Numerisk studie av närfält kring matematiskt tunna vingar med lyftkraft," M.E. thesis 1976, Teknikum/Uppsala University, Sweden. (The work was done at Saab-Scania in 1976).

17 Drougge, G., "An experimental investigation of the interference between bodies of revolution at transonic speeds with special reference to the sonic and supersonic area rules," The Aeronautical Research Inst. of Sweden, Report 83, Stockholm 1959.

18 Andrews, D. R. et al., "Flight measurements of the drag of an aircraft fitted with a rear fuselage fairing designed to reduce the transonic drag," A.R.C. Technical Report C.P. No. 459 (Report No. Aero 2580, Nov. 1956).

19 Berndt, S. B., "On the drag of slender bodies at sonic speed," The Aeronautical Inst. of Sweden, FFA Report 70, Stockholm May 1955.

20 Karlsson, K. R., "Numerisk studie av när- och fjärrfält kring slanka kroppskonfigurationer i underljudsströmning," M.E. thesis 1974, Technical faculty/Linköping University, Sweden (The work was done at Saab-Scania in 1973-74).

21 Stahara, S. S. and Spreiter, J. R., "Calculative Techniques for transonic flows about certain classes of wing-body combinations, Phase II", NASA CR-2157, Dec. 1972.

ACKNOWLEDGEMENTS

The work described in this paper has been supported by the Air Material Department of the Swedish Defence Material Administration.

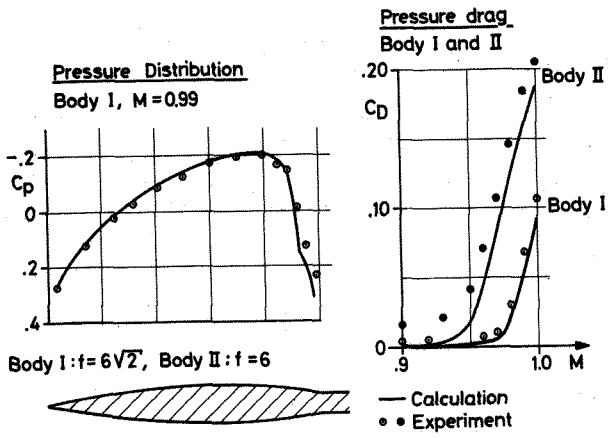

Fig 4. PARABOLIC ARC BODIES

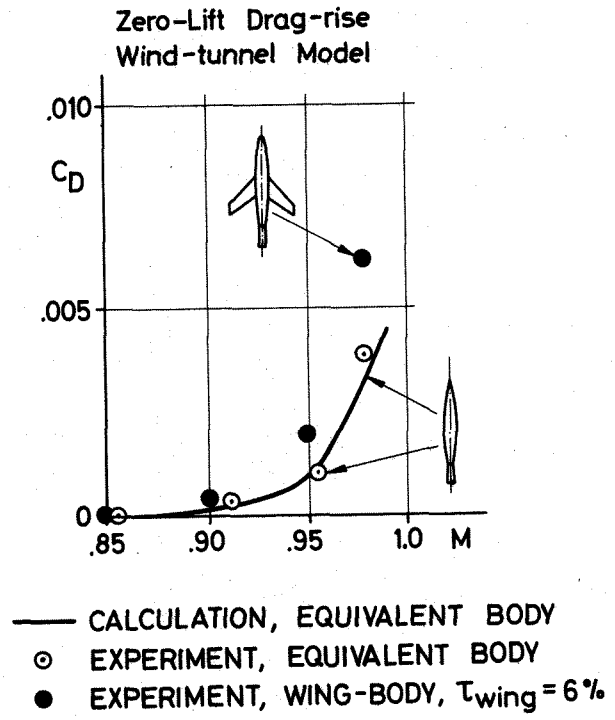

Fig 5. WING-BODY COMBINATION

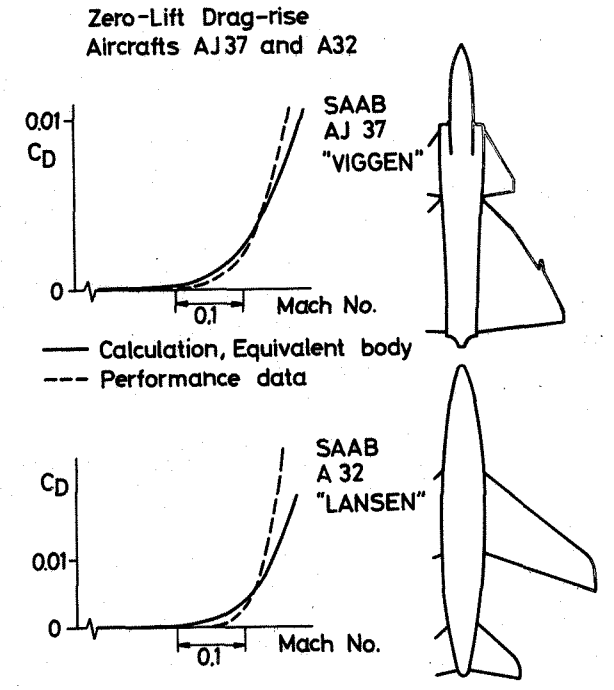

Fig 6. CANARD-DELTA AND SWEPT WING-TAIL CONFIGURATIONS

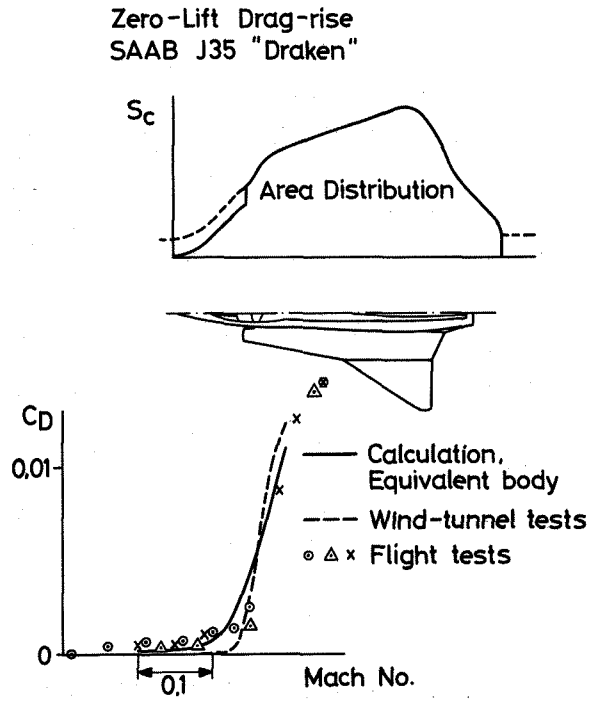

Fig 7. DELTA-WING CONFIGURATION

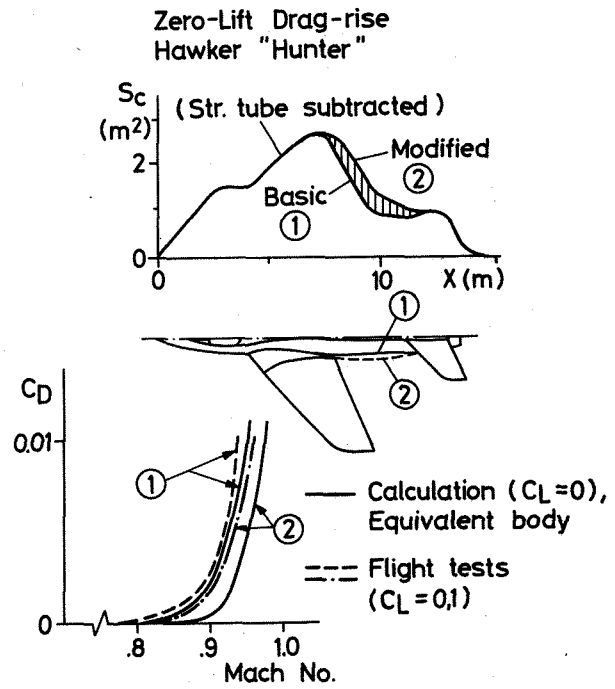

Fig 9. SLENDER SWEPT WING-TAIL COMBINATION

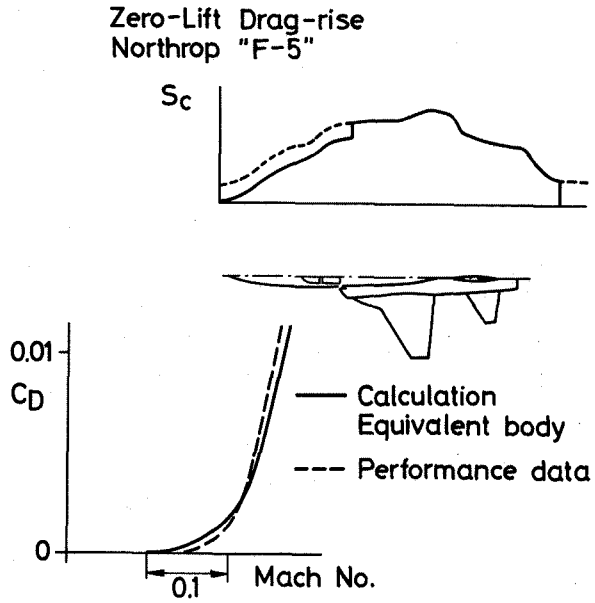

Fig 8. SLENDER WING-TAIL COMBINATION

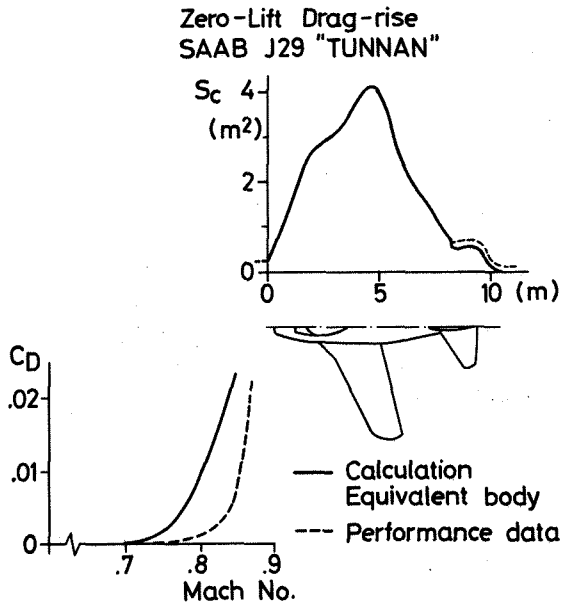

Fig 10. THICK SWEPT WING-TAIL COMBINATION

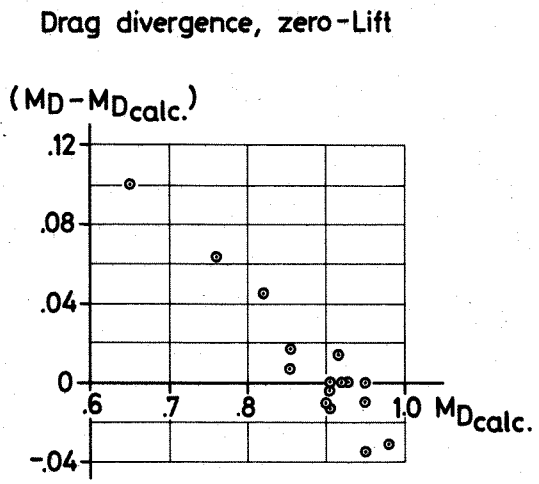

Fig 11. DRAG DIVERGENCE CORRELATION

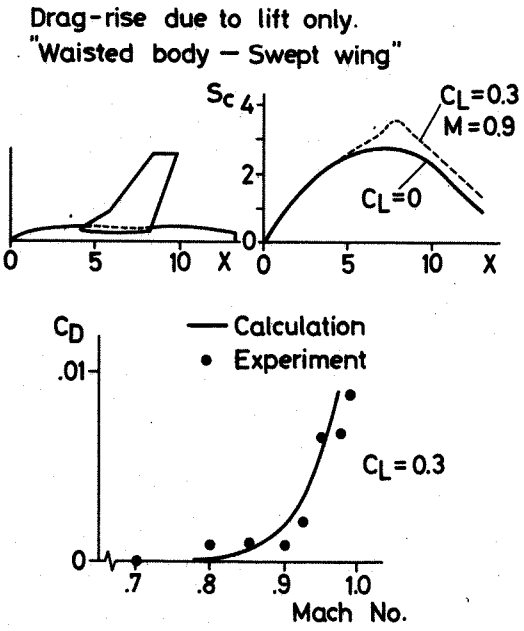

Fig 12. DRAG-RISE DUE TO LIFT, WAISTED BODY-SWEPT WING

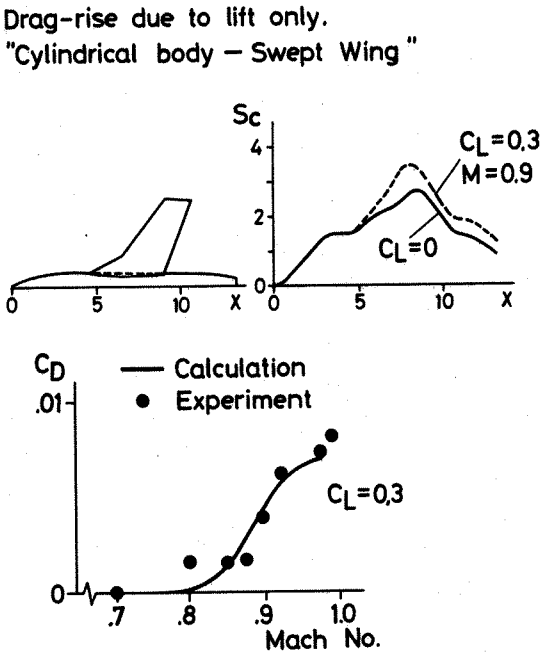

Fig 13. DRAG RISE DUE TO LIFT, CYLINDRICAL BODY-SWEPT WING

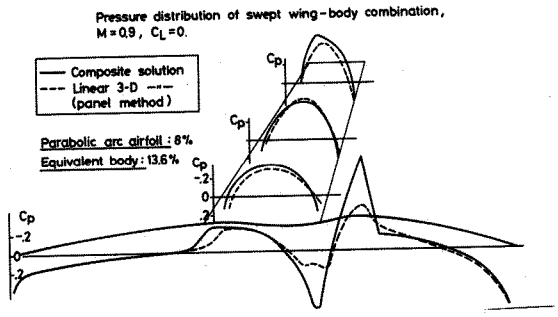

Fig 14. COMPOSITE SOLUTION CONTRA LINEAR THREE-DIMENSIONAL THEORY

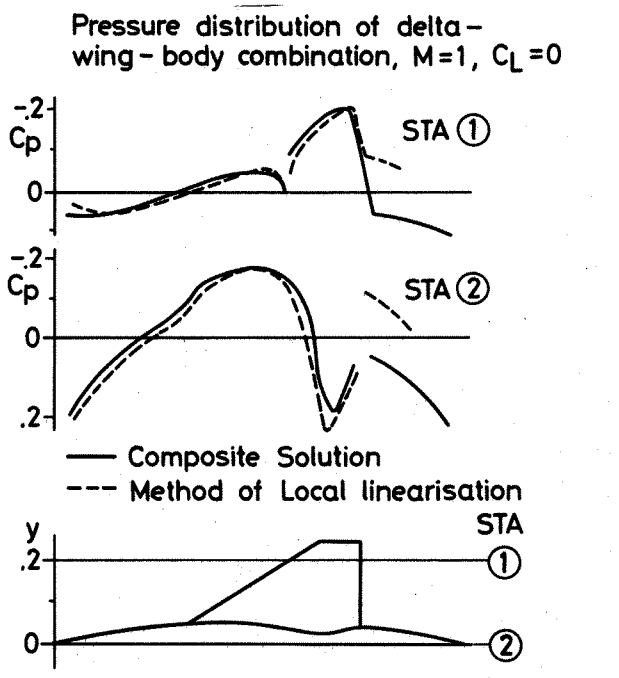

Fig 15. COMPOSITE SOLUTION CONTRA METHOD OF LOCAL LINEARISATION